Supporting Online Material

Materials and Methods

Cell lines and cell culture. The mouse cell lines and their characteristics are listed in Table S1. Low metastatic P29 and high metastatic A11 cells originated from Lewis lung carcinoma, but express different metastatic potentials (*21*, *22*). Low metastatic B82 cells, derived from the L929 fibroblast cell line (C3H/An mouse strain), are deficient in thymidine kinase, resulting in simultaneous expression of BrdU-resistant and HAT-sensitive phenotypes (*S1*). B82 cells express tumorigenicity probably due to spontaneous transformation. In this study, high metastatic B82M cells were isolated from a lung nodule formed by the injection of low metastatic B82 cells into the tail vein of nude mice. The 13885insC mutation in *ND6*, which is found in the mtDNA of B82M cells (Table 1), has been reported previously (*S2, S3*) as a pathogenic mutation inducing significant complex I defects in some sublines of an L929 fibroblast cell line and A9 cells derived from the L929 line. We also used another pair of tumor cells with low metastatic potential (NM11) and high metastatic potential (LuM1) derived from murine colon adenocarcinoma 26 (kindly provided from Dr. S. Shimizu, Aichi Cancer Center Research Institute, Japan) (*S4*). NIH3T3 cells were derived from NIH/Swiss mouse embryos as non-transformed fibroblasts, which do not form tumors after inoculation under the skin of nude mice (*S5*). We also used two human tumor cell lines, low metastatic HeLa cells and high metastatic MDA-MB-231 cells. Parental cells, their ρ^0 cells, and the cybrids were grown in normal medium [DMEM + pyruvate (0.1 mg/ml) + uridine (50 mg/ml) + 10% fetal bovine serum]. Hypoxic culture conditions (< 2% O_2) were generated in a BBL GasPak Pouch (Becton Dickinson Microbiology Systems, Cockeysville, MA, USA).

Isolation of trans-mitochondrial cybrids. We isolated ρ^0 cells by treating parental cells with 1.5 mg/ml ditercalinium (DC), an antitumor bis-intercalating agent (*S6*). Complete depletion of mtDNA was confirmed by PCR analysis. Plasmid pSV2neo was furthermore transfected into ρ^0 P29 and ρ^0 A11 cells to be resistant to G418. Enucleated cells of the mtDNA donor were prepared by their pretreatment with cytochalasin B (10 μg/ml) for 2 min and centrifugation at 7,500 × *g* for 10 min. Resultant cytoplasts were fused with ρ^0 cells by polyethylene glycol. Selective isolation of these cybrids was attained in the selection medium with G418 and without uridine and pyruvate (UP^-), so that we could exclude mtDNA donors by G418 selection, and unfused nuclear donor ρ^0 cells by UP^- selection. The selection medium with BrdU or HAT was used for isolation of the cybrids with or without B82 nuclear DNA (cf. Table S2). We also isolated human cybrids by the fusion of ρ^0 HeLa cells, which are deficient in mtDNA and resistant to 6-thioguanine (TG) (*S7*), with enucleated MDA-MB-231 cells, followed by selection with UP^- and TG for excluding unfused parental ρ^0 HeLa cells and MDA-MB-231 cells, respectively. Therefore, they carry nuclear DNA from ρ^0 HeLa cells and mtDNA from enucleated MDA-MB-231 cells. As control cybrids, we used the HemtHe cybrids carrying nuclear DNA from ρ^0 HeLa cells and mtDNA from wild-type HeLa cells (*S8*). They were isolated by the fusion of ρ^0 HeLa cells

with enucleated wild-type HeLa cells that are sensitive to TG, followed by selection with UP^- and TG for excluding unfused parental ρ^0 HeLa cells and wild-type HeLa cells, respectively.

Biochemical measurement of respiratory enzyme activities. Cells in log-phase growth were harvested, and the mitochondrial respiratory function was assayed as described before (*S9*). Briefly, NADH and cytochrome *c* (oxidized form) were used as substrates for estimation of complexes I + III activity, and the reduction of cytochrome *c* was monitored at 550 nm. For estimation of complexes II + III activity, sodium succinate and cytochrome *c* (oxidized form) were used as substrates, and reduction of cytochrome *c* was monitored at 550 nm.

Measurement of ROS production. ROS generation was detected with 2′-,7′-dichlorofluorescein diacetate (DCFH-DA) (Invitrogen, Carlsbad, CA, USA) and mitochondrial superoxide indicator MitoSOX-RED (Invitrogen). Cells were incubated with 5 μM DCFH-DA or with 5 μM MitoSOX-RED for 10 min at 37 ºC in serum-free DMEM, washed twice with Dulbecco's phosphate-buffered saline (DPBS), and then immediately analyzed with a FACScan flow cytometer (Becton Dickinson, Mountain View, CA, USA).

Sequencing of mtDNAs. Total DNAs extracted from 2×10^5 P29, A11, B82 and B82M cells, respectively, were used for amplification of mtDNA fragments. The PCR reactions amplified 2.5-3.0 kbp mtDNA fragments using eight primer pairs designed to generate overlapping fragments of mtDNA. The nucleotide positions used as oligonucleotide primers were as follows: fragment 1 (n.p. 2,045 to 2,064 and 4,623 to 4,603), fragment 2 (n.p. 4,058 to 4,077 and 6,568 to 6,549), fragment 3 (n.p. 5,931 to 5,950 and 8,626 to 8,606), fragment 4 (n.p. 8,050 to 8,069 and 11,008 to 10,989), fragment 5 (n.p. 10,370 to 10,390 and 12,972 to 12,953), fragment 6 (n.p. 12,394 to 12,413 and 15,087 to 15,068), fragment 7 (n.p. 14,426 to 14,445 and 654 to 635), fragment 8 (n.p. 72 to 91 and 2,735 to 2,716). All PCR amplifications were performed in a 50 μl of solution consisting of 1 × PCR buffer, 0.2 mM dNTPs, 0.6 μM primers, 1 U Ampli Taq Gold DNA polymerase (Applied Biosystems, Foster City, CA, USA), and 1 μg of cellular DNA as template. Reaction conditions were 95 °C for 10 min with cycle times of 60 s for denaturation at 95 °C, 60 sec for annealing at 50-56 °C, and 150 s for extension at 72 °C for 35 cycles. The final extension was for 10 min. Amplified mtDNA fragments were separated in 1.0% agarose gel and extracted, and then directly sequenced.

Genotyping of mtDNAs. Replacement of mtDNAs in the cybrids was confirmed by RFLP analysis of the PCR products. For recognition of the G13997A mutation, a 147 bp-fragment containing the 13,997 site was amplified by PCR. The nucleotide sequences from n.p. 13,963 to 13,996 (CCCACTAACAATTAAACCTAAACCTCCATActTA, small letters indicate the mismatch site) and n.p. 14,109 to 14,076 (TTCATGTCATTGGTCGCAGTTGAATGCTGTGTAG) were used as oligonucleotide primers. Combination of the PCR-generated mutation with the G13997A mutation creates a restriction site for

Afl II, and generates 114-bp and 33-bp fragments on *Afl* II digestion. The restriction fragments were separated in 3% agarose gel.

For recognition of the 13885insC mutation, a 147-bp-fragment containing the 13,885 site was amplified by PCR. The nucleotide sequences from n.p. 13,772 to 13,792 (ACCTCTATAATCACCCCCAAT) and n.p. 13,918 to 13,887 (GGTTTAATAGTTTTTTTAATTTATTTAGGaGG, small letters indicate the mismatch site) were used as oligonucleotide primers. Combination of the PCR-generated mutation with the 13885insC mutation creates a restriction site for *BsaX* I, and generates 100-, 30-, and 17-bp fragments on *BsaX* I digestion. Because *BsaX* I cuts 2 spots per 1 recognition site, the amplified products with the 13885insC mutation generate 3 fragments. The restriction fragments were separated in 3% agarose gel.

Assays of metastatic potential and tumorigenicity. For testing experimental and spontaneous metastatic potential, 5×10^5 cells and 5×10^6 cells/100 μl PBS were injected into the tail vein and under the back skin, respectively, of 6-week-old male C57BL/6 mice (CLEA Japan, Tokyo, Japan). The mice were sacrificed 18 days later (for experimental metastasis) or 25 to 38 days later depending on the *in vivo* growth of each cybrid (for spontaneous metastasis), and their lungs were removed. The lungs were fixed in the Bouin's solution, and parietal nodules were counted. For examination of the effect of NAC administration on spontaneous metastatic potential, the mice were given 10 mg/ml NAC in drinking water *ad libitum*. For determination of tumorigenicity, growing cells (5×10^6 cells) suspended in 100 μl PBS were injected subcutaneously into the back of 5-week-old male C57BL/6 mice. Tumor growth was monitored assuming spherical growth of tumors. When a tumor mass was detectable visually, its maximum (*a*) and minimum (*b*) diameters and height (*h*) were recorded twice per week. The volume of each tumor (*V*) was calculated according to the formula: $V = \pi abh/6$.

SDS-PAGE and Western blotting. For detecting MCL-1, cells were lysed on ice for 10 min in 1% Triton X-100, 1% sodium deoxycholate, 0.1% SDS, 50 mM Tris-HCl (pH 7.5), 150 mM NaCl, 1 mM PMSF, and protease inhibitor cocktail (Sigma-Aldrich, St. Louis, MO, USA). After centrifugation at $10,000 \times g$ for 10 min at 4 ºC, the supernatant was used as a sample. For detecting HIF-1α, nuclear extracts prepared with a Nuclear Extract Kit (ACTIVE MOTIF, Carlsbad, CA, USA) were used. Proteins were resolved by SDS-PAGE under reducing conditions. The resolved proteins were transferred electrophoretically to a nitrocellulose membrane. After incubation with 5% dry milk in TBS-T (150 mM NaCl, 50 mM Tris-HCl (pH 7.4), 0.05% Tween 20) for at least 1 h at room temperature, the membrane was incubated with polyclonal anti-MCL-1 antibody (Santa Cruz Biotechnologies, Inc., Santa Cruz, CA, USA) or monoclonal anti-HIF-1α antibody (Novus Biologicals, Kittketon, CO, USA) for 1 h at room temperature or overnight at 4 ºC, washed extensively with TBS-T, and then incubated with horseradish peroxidase-conjugated goat anti-rabbit or goat anti-mouse IgG, respectively. Proteins were detected using ECL Western blotting detection reagents (Amersham Biosciences Corp., Piscataway, NJ, USA). For loading controls, the membrane was stripped, and subsequently incubated with

monoclonal anti-β-actin antibody (Sigma-Aldrich) or polyclonal anti-E2F-1 antibody (Santa Cruz Biotechnologies) followed by incubation with horseradish peroxidase-conjugated goat anti-mouse or goat anti-rabbit IgG, respectively.

VEGF quantification. Cells were seeded at 1×10^5 cells/well in a 12-well plate and cultured for 24 h under normoxic or hypoxic conditions. Cell supernatants were collected, and concomitantly, cells were harvested by trypsinization, and their cell number was determined. The amount of VEGF in the supernatant was measured with an enzyme-linked immunosorbent assay kit (Quantikine, R&D Systems, Mineapolis, MN, USA). VEGF was expressed as picograms of VEGF/10^5 cells/24 h.

Transfection of *Mcl-1* siRNA. Silencer negative Control #1 siRNA (Ambion Inc., Austin, TX, USA) or *Mcl-1* siRNA (Santa Cruz Biotechnologies) was transfected into cells with Lipofectamin 2000 (Invitrogen). As a mock transfection, cells were incubated with Lipofectamin 2000 only. Three days after transfection, the cells were subjected to immunoblot analysis for MCL-1 expression and experimental metastasis assay.

Measurement of the concentration of lactate in the cell medium. Cells were seeded at 5×10^4 cells/well of a 6-well plate and cultured for 24 h. The amounts of lactate in the cell medium were estimated using an F-kit $_L$-Lactic acid (Roche, Basel, Switzerland).

RNA extraction and semi-quantitative RT-PCR analysis of glycolytic gene expression. Total RNA was extracted by using QIAGEN RNeasy Protect Mini Kit. One microgram of total RNA was reverse-transcribed into cDNA, and the resulting cDNA was used for amplification of target cDNAs using *Go*Taq DNA polymerase (Promega Corp., Madison, WI, USA). The sense and antisense oligonucleotides used for PCR were: 5′- CCTGCTCGTATTGCTGTGGCTGGC-3′ and 5′-GGAAGAGGTCTCATCTAGC TGCCT-3′ for glucose transporter-1 (*Glut-1*), and 5′-ACCACAGTCCATGCCATCAC-3′ and 5′-TCCACCACCCTGTTGCTGTA-3′ for glyceraldehyde-3-phosphate dehydrogenase (*GAPDH*), respectively. The PCR conditions were: 94°C for 5 min, and then 23 cycles with 94°C for 10 s, 55°C for 10 s, 72°C for 30 s, and 72°C for 5 min.

Microarray analysis. Total RNA was extracted from log-phase cultures of the P29mtP29, P29mtA11, A11mtP29, and A11mtA11 cybrids, then cRNA and cDNA targets were prepared following the standard protocol of "Eukaryotic Sample and Array Processing" (Affymetrix, Santa Clara, CA, USA; see https://www.affymetrix.com/support/downloads/manuals/expression_s2_manual.pdf). Hybridizations of cRNA and cDNA targets were performed according to the manufacturer's recommended procedures on high-density oligonucleotide gene chips (Affymetrix Mouse Genome 430 2.0 GeneChip arrays). Differences in gene

expression between P29mtP29 and P29mtA11 and between A11mtP29 and A11mtA11 were analyzed using GeneChip Operating Software ver. 1.4 (Affymetrix).

Statistical Analysis. The data were analysed with a Student's *t* test. All values are the mean ± s.d., and values with $P < 0.05$ were considered significant.

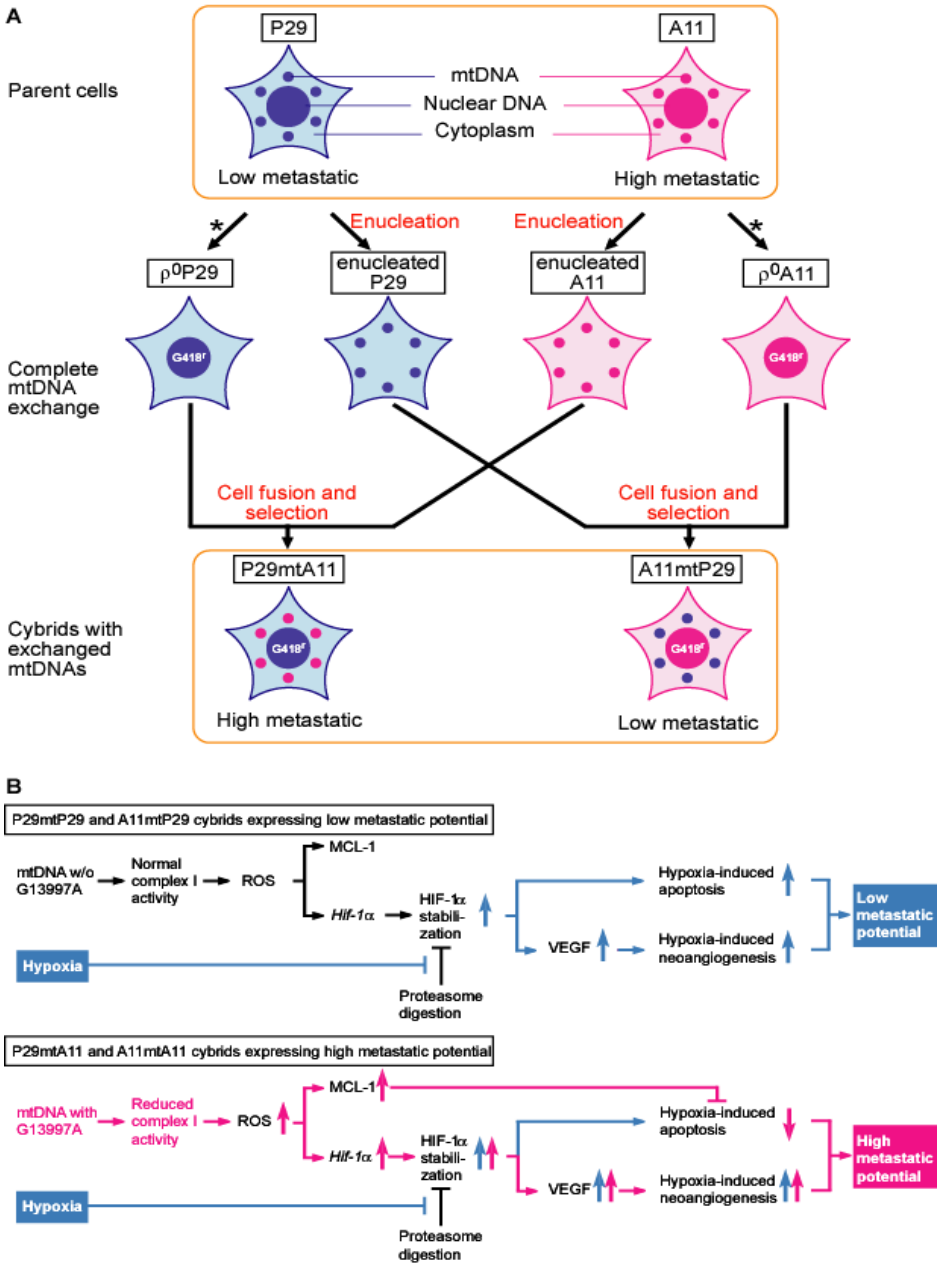

Supporting Figure 1 Schemes for isolation and characterization of trans-mitochondrial cybrids carrying completely exchanged mtDNA between low metastatic P29 cells and high metastatic A11 cells.

(**A**) Scheme for the isolation of cybrids with completely exchanged mtDNA. *, Parental P29 and A11 cells were treated with ditercalinium for isolation of ρ^0P29 and ρ^0A11 cells, which have no mtDNA, and then the G418-resistance plasmid was introduced into the ρ^0P29 and ρ^0A11 cells to permit isolation of ρ^0 cells resistant to G418. High metastatic potential is transferred with the transfer of mtDNA from the A11 cells, and low metastatic potential is transferred with the transfer of mtDNA from the P29 cells. Involvement of cytoplasmic factors other than mtDNA from the A11 cells in expression of the high metastatic potential in the P29mtA11 cybrids can be ruled out by the observations that the A11mtP29 cybrids lost their high metastatic potential, even though they always contain cytoplasmic factors transcribed by the nuclear genes derived from the A11 cells. (**B**) Metabolic scheme that illustrates how the G13997A mtDNA from high metastatic A11 cells reversibly controls high metastatic potential. Blue lines, arrows, and characters are hypoxia-induced changes, whereas red ones represent changes induced by the G13997A mtDNA from the A11 cells.

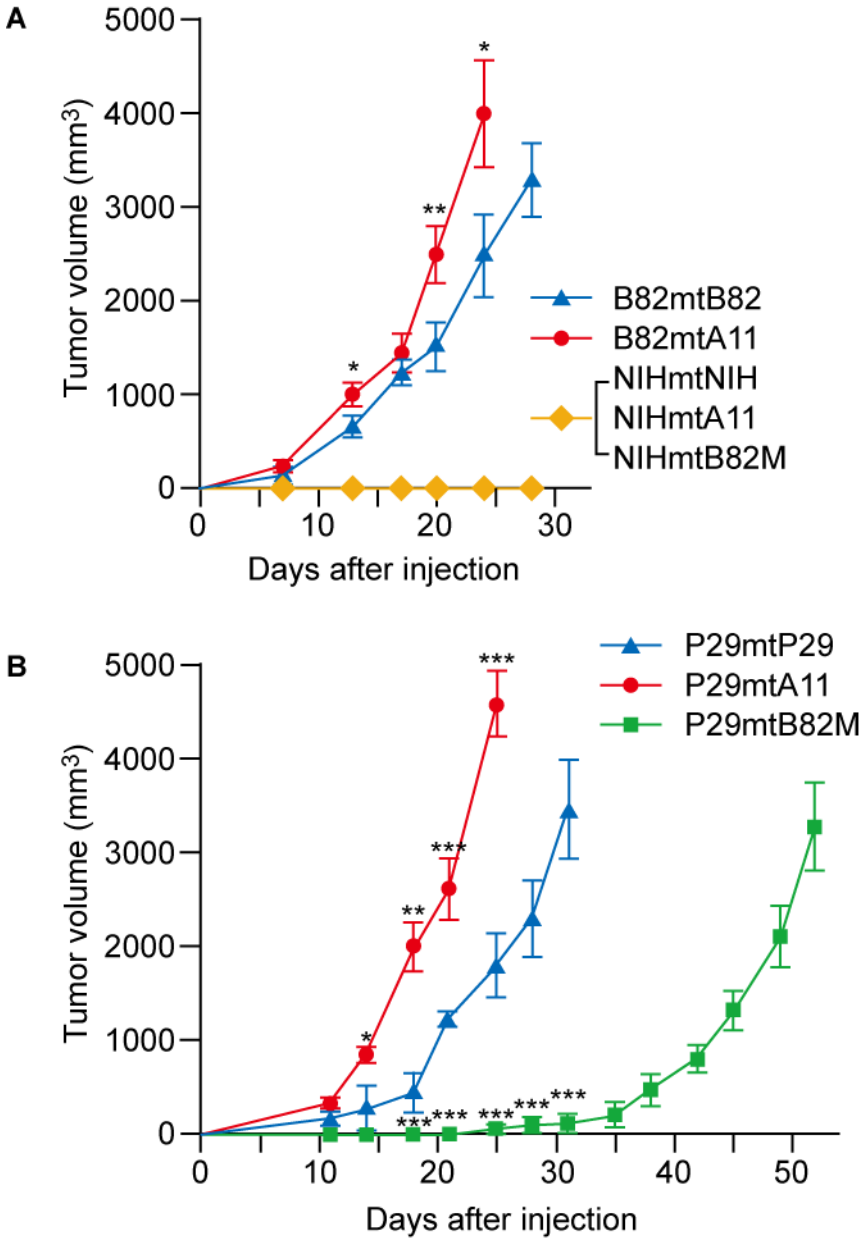

Supporting Figure 2 Growth of primary tumors in (A) nude mice and (B) C57BL/6 mice.

The P29mtA11 cybrids, which express high metastatic potential, grew faster as primary tumors than the P29mtP29 cybrids, which express low metastatic potential. In contrast, the P29mtB82M cybrids, which express high metastatic potential, showed slower growth as primary tumors than the P29mtP29 cybrids. Thus, the expression of the high metastatic potential does not necessarily correlate with the growth rate of the primary tumors. *, $P < 0.05$, **, $P < 0.01$, and ***, $P < 0.001$, relative to B82mtB82 (**A**) or P29mtP29 (**B**).

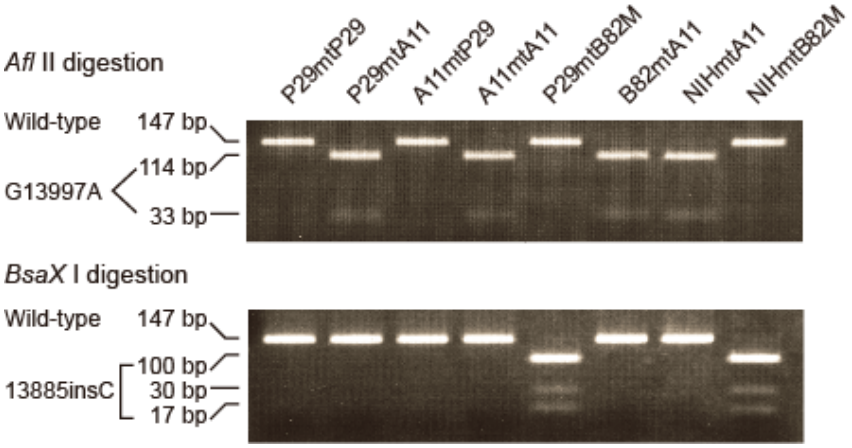

Supporting Figure 3 Identification of the mtDNA genotypes by means of restriction enzyme digestion of the PCR products.

The PCR products of the mtDNA with the G13997A mutation from A11 cells produce 114- and 33-bp fragments because of the gain of an *Afl* II site by a G13997A substitution, whereas those of mtDNA without the mutation produce a 147-bp fragment due to the absence of the *Afl* II site. For recognition of the 13885insC mutation, a 147-bp fragment containing the 13,885 site was amplified by PCR using mismatched primers. PCR products with the 13885insC mutation create a restriction site for *BsaX* I, and generated 100-, 30-, and 17-bp fragments.

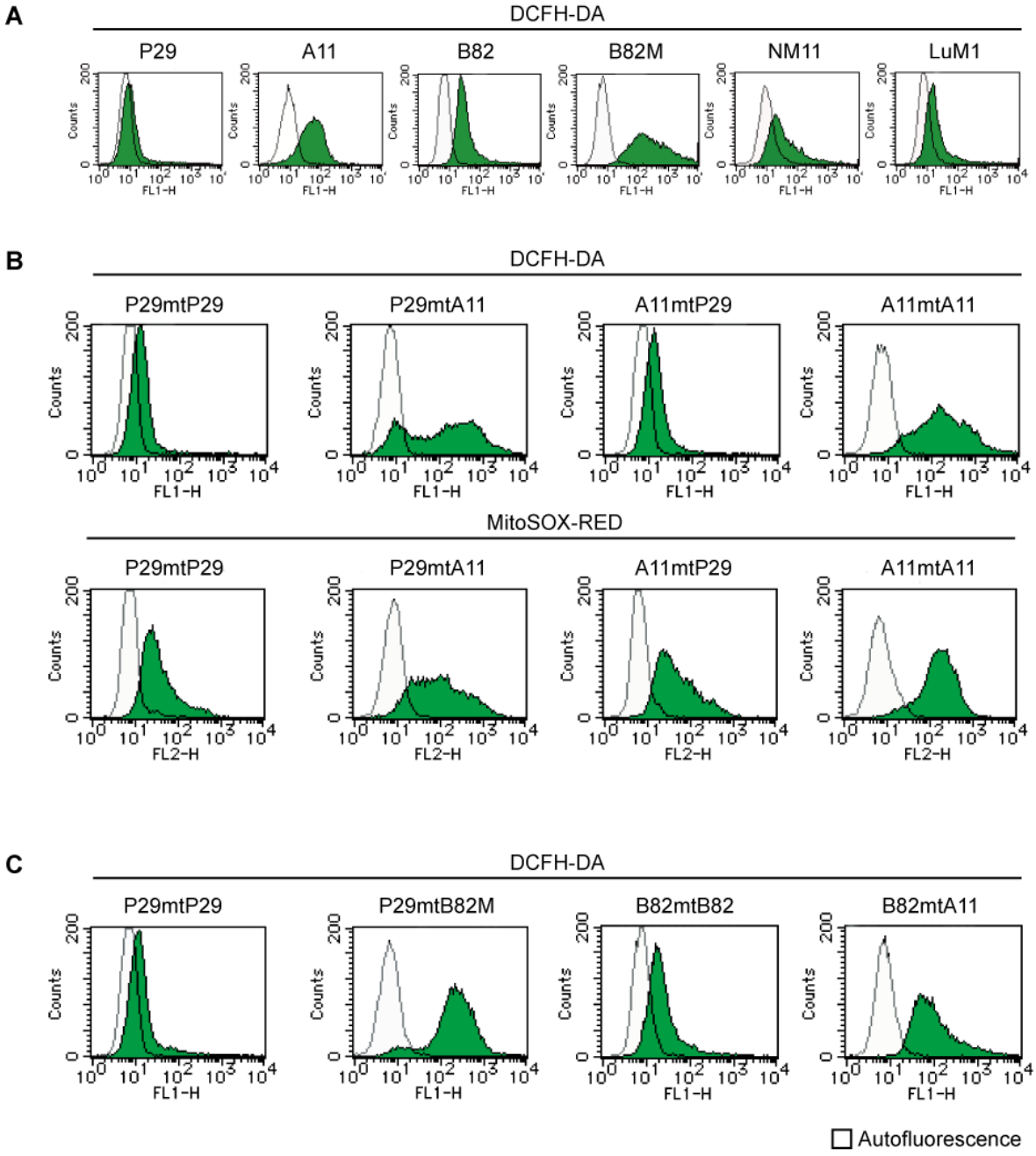

Supporting Figure 4 Effects of the complex I defects in the cybrids on ROS production.

To estimate ROS production, we carried out flow-cytometric analysis using 1×10^6 cells. (**A**) Parent cells treated with 5 μM DCFH-DA were subjected to FACScan for quantitative estimation of H_2O_2. (**B**) Cybrids with exchanged mtDNA between P29 and A11 cells were treated with 5 μM DCFH-DA (upper panels) and 5 μM MitoSOX-RED (lower panels) and subjected to FACScan for quantitative estimation of H_2O_2 and superoxide, respectively. (**C**) The P29mtP29, P29mtB82M, B82mtB82, and B82mtA11 cybrids treated with 5 μM DCFH-DA were subjected to FACScan for quantitative estimation of H_2O_2.

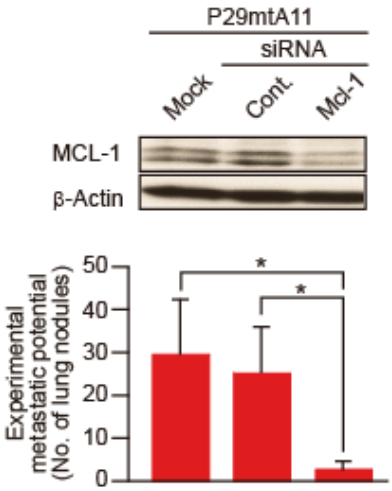

Supporting Figure 5 Effects of knockdown of MCL-1 by siRNA on metastatic potential.

Mock-transfected P29mtA11 cybrids and cybrids transfected with 50 nM control or *Mcl-1* siRNA were subjected to Western blots for MCL-1 expression (upper panel), and metastasis assays (lower panel). Bars represent the mean ± s.d. (n = 7). *, $P < 0.02$.

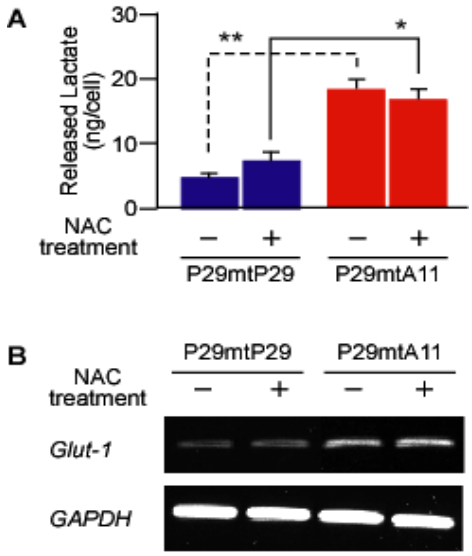

Supporting Figure 6 Effects of NAC treatment on the glycolytic activity of the P29mtP29 and P29mtA11 cybrids.

The effects of NAC treatment of the P29mtP29 and P29mtA11 cybrids on (**A**) the lactate level and (**B**) the expression of glucose transporter-1 (*Glut-1*). The cybrids were treated with 20 mM NAC for 24 h. The P29mtA11 cybrids showed enhanced lactate level in culture medium and upregulation of *Glut-1* compared to the P29mtP29 cybrids, suggesting that enhanced glycolytic activity in the P29mtA11 cybrids results from complex I defects. The P29mtP29 cybrids were treated as the cybrids with normal mitochondrial respiratory function and normal glycolytic activity. Bars represent the mean ± s.d. (n = 3). *, $P < 0.02$; **, $P < 0.01$.

Supporting Table 1 Characteristics of mouse cell lines used for mtDNA replacement

Mouse cell lines*[1]	Cell type	Mouse strain	Drug resistance*[2]	mtDNA	Metastatic potential
P29	Lewis lung carcinoma	C57BL/6	-	+	Low
A11	Lewis lung carcinoma	C57BL/6	-	+	High
B82	Fibrosarcoma	C3H/An	$BrdU^{r}$*[4]=HAT^{s}*[4]	+	Low
B82M	Fibrosarcoma	C3H/An	$BrdU^{r}$=HAT^{s}	+	High
NM11	Colon cancer	BALB/c	-	+	Low
LuM1	Colon cancer	BALB/c	-	+	High
NIH3T3	Non-transformed fibroblasts	NIH/Swiss	-	+	
ρ^{0}*[3]P29	Lewis lung carcinoma	C57BL/6	$G418^{r}$, UP^{-s}	-	
ρ^{0}A11	Lewis lung carcinoma	C57BL/6	$G418^{r}$, UP^{-s}	-	
ρ^{0}B82	Fibrosarcoma	C3H/An	$BrdU^{r}$=HAT^{s}, UP^{-s}	-	
ρ^{0}NIH3T3	Non-transformed fibroblasts	NIH/Swiss	UP^{-s}	-	

*[1] The origins of the cell lines are described in the Materials and Methods.

*[2] BrdU, bromodeoxyuridine; HAT, hypoxanthine/aminopterin/thymidine; G418, geneticin analogue; UP^{-}, without uridine and pyruvate.

*[3] ρ^{0} cells represent mtDNA-less cells.

*[4] ^{r} and ^{s} represent resistant and senstitive to each drugs, respectively.

Supporting Table 2 Isolation of the trans-mitochondrial cybrids and their metastatic characteristics

Cybrids	Fusion combination			Selection	Tumori-genicity*1	Metastatic potential*2	
	Nuclear donors	×	mtDNA donors			Exp.*3 rate*5	Spont.*4 rate*5
P29mtP29	ρ^0*6P29	×	en*6P29	G418+UP$^-$	+	0 / 6	0 / 8
P29mtA11	ρ^0P29	×	enA11	G418+UP$^-$	+	8 / 8	8 / 8
A11mtP29	ρ^0A11	×	enP29	G418+UP$^-$	+	0 / 6	0 / 8
A11mtA11	ρ^0A11	×	enA11	G418+UP$^-$	+	12 / 12	8 / 8
P29mtB82M	ρ^0P29	×	enB82M	HAT+UP$^-$	+	6 / 6	
B82mtB82	ρ^0B82	×	enP29mtB82*7	BrdU+UP$^-$	+	0 / 6	
B82mtA11	ρ^0B82	×	enA11	BrdU+UP$^-$	+	6 / 6	
NIHmtNIH	ρ^0NIH3T3	×	enB82mtNIH*7	HAT+UP$^-$	-	0 / 6	
NIHmtA11	ρ^0NIH3T3	×	enB82mtA11	HAT+UP$^-$	-	0 / 6	
NIHmtB82M	ρ^0NIH3T3	×	enB82M	HAT+UP$^-$	-	0 / 6	

*1 We examined tumorigenicity of the cybrids with nuclear DNA from P29 and A11 cells and from B82 and NIH3T3 cells by inoculation of 5×10^6 cells under the skin of C57BL/6 mice and nude mice, respectively. Tumor growth was shown in Fig. S2.

*2 We showed metastatic potential by examination of experimental and spontaneous metastasis. Experiments were repeated at least 3 times.

*3 Experimental metastasis (Exp.) of the cybrids with nuclear DNA from P29 and A11 cells and from B82 and NIH3T3 cells was examined by counting the number of lung nodules in C57BL/6 mice and nude mice, respectively, at 18 days after inoculation of 5×10^5 cells into tail vein. P29mtA11, P29mtB82M and A11mtA11 cybrids formed 28.7 ± 5.1, 73.3 ± 6.8, and 69.4 ± 7.9 nodules per lung, respectively. B82mtA11 cybrids formed 21 ± 5.8 nodules per lung.

*4 Spontaneous metastasis (Spont.) was examined by counting the number of lung nodules in C57BL/6 mice when primary tumor size of each cybrid group reached approximately the same volume (5 cm^3) at 25 and 38 days after inoculation of 5×10^6 cells under the skin of the back. While the cybrids with mtDNA from P29 cells (i.e. P29mtP29 and A11mtP29 cybrids) did not form lung nodules, the cybrids with mtDNA from A11 cells (i.e. P29mtA11 and A11mtA11 cybrids) formed 2.6 ± 1.2 (n =8) and 12.4 ± 8.5 (n =8) lung nodules, respectively. The difference between the cybrids with mtDNA from A11 and the cybrids with mtDNA from P29 was statistically significant (P < 0.0001, Mann-Whitney U-test).

*5 No. of mice with lung nodules/no. of mice injected.

*6 ρ^0 represents mtDNA-less, en represents enucleated.

*7 P29mtB82 cybrids were isolated by the fusion of ρ^0P29 with enucleated B82 cells, and subsequent selection with HAT + UP$^-$ medium. B82mtNIH cybrids were isolated by the fusion of ρ^0B82 with enucleated NIH3T3 cells, and subsequent selection with BrdU + UP$^-$ medium.

Supporting Table 3 Gene expression profiles in cybrids with P29 mtDNA and cybrids with A11 mtDNA

Ontology	Gene Symbol	Gene Title	Entrez Gene ID	Ratio (log_2)*[1]	
				P29mtA11 /P29mtP29	A11mtA11 /A11mtP29
Glycolysis pathway	Aldoa-ps2	aldolase 1, A isoform, pseudogene 2	353204	1.5	4.3
	Dhtkd1	dehydrogenase E1 and transketolase domain containing 1	209692	1.1	3.6
	Gck	glucokinase	103988	2.3	1.6
	Hkdc1	hexokinase domain containing 1	216019	3.7	1.2
Glucose transport	Slc2a3	solute carrier family 2 (facilitated glucose transporter), member 3	20527	2.3	4.0
Angiogenesis	Anpep	alanyl (membrane) aminopeptidase	16790	1.8	4.9
	Kdr	kinase insert domain protein receptor	16542	3.5	1.7
	Flt1	FMS-like tyrosine kinase 1	14254	-2.1	-3.2
	Pgf	placental growth factor	18654	-1.5	-3.0
Apoptosis	Aatk	apoptosis-associated tyrosine kinase	11302	2.8	1.2
	Birc1b	baculoviral IAP repeat-containing 1b	17948	1.2	1.7
	Birc1e	baculoviral IAP repeat-containing 1e	17951	1.7	3.0
	Birc3	baculoviral IAP repeat-containing 3	11796	3.2	4.3
	Card4	caspase recruitment domain 4	107607	3.0	4.1
	Casp1	caspase 1	12362	2.1	2.0
	Faim2	Fas apoptotic inhibitory molecule 2	72393	2.4	5.3
	Lgals7	lectin, galactose binding, soluble 7	16858	2.8	2.7
	Lhx4	LIM homeobox protein 4	16872	1.5	1.0
	Mcl1	myeloid cell leukemia sequence 1	17210	1.0 *[2]	1.7 *[2]
	Mycs	myc-like oncogene, s-myc protein	17870	3.3	1.9
	Plg	plasminogen	18815	2.7	1.8
	Tnfrsf21	tumor necrosis factor receptor superfamily, member 21	94185	-1.2	-2.0
Cell adhesion	1110049B09Rik	RIKEN cDNA 1110049B09 gene	68764	1.0	1.6
	3110041P15Rik	RIKEN cDNA 3110041P15 gene	73159	1.4	1.5
	Agc1	aggrecan 1	11595	3.2	2.0
	Cd97	CD97 antigen	26364	4.6	1.7
	Cdh20	cadherin 20	23836	1.7	2.1
	Cdh26	cadherin-like 26	381409	1.8	1.4
	Cldn23	claudin 23	71908	3.2	2.6
	Col10a1	procollagen, type X, alpha 1	12813	3.4	2.9
	Col5a2	procollagen, type V, alpha 2	12832	2.9	2.0
	Col5a3	procollagen, type V, alpha 3	53867	2.5	2.6
	Col6a1	procollagen, type VI, alpha 1	12833	1.6	2.0
	Col6a2	procollagen, type VI, alpha 2	12834	4.1	2.5
	Col6a3	procollagen, type VI, alpha 3	12835	5.2	3.7
	Col8a2	procollagen, type VIII, alpha 2	329941	3.1	2.4
	Emilin2	elastin microfibril interfacer 2	246707	1.9	3.5
	Fcgbp	Fc fragment of IgG binding protein	215384	1.0	1.3
	Frem2	Fras1 related extracellular matrix protein 2	242022	3.4	1.9
	Gp1ba	glycoprotein 1b, alpha polypeptide	14723	1.6	3.7
	Gp5	glycoprotein 5 (platelet)	14729	1.0	1.0
	Icam4	intercellular adhesion molecule 4, Landsteiner-Wiener blood group	78369	2.8	2.1
	Itgb2	integrin beta 2	16414	2.4	1.6

Cell adhesion	Itgb3	Integrin beta 3 (Itgb3), mRNA	16416	5.0	2.0
	L1cam	L1 cell adhesion molecule	16728	2.4	5.9
	Mcam	melanoma cell adhesion molecule	84004	1.4	1.0
	Pcdhb1	protocadherin beta 1	93872	2.7	2.0
	Pcdhb8	protocadherin beta 8	93879	1.8	1.2
	Pecam1	platelet/endothelial cell adhesion molecule 1	18613	2.5	2.8
	Pkp3	plakophilin 3	56460	1.5	2.8
	Reln	Reelin (Reln), mRNA	19699	2.4	2.0
	Siglec5	sialic acid binding Ig-like lectin 5	233186	4.0	1.4
	Stab1	stabilin 1	192187	3.3	2.4
	Vwf	Von Willebrand factor homolog	22371	1.6	1.7
	Lama1	laminin, alpha 1	16772	-1.6	-2.4
	Alcam	activated leukocyte cell adhesion molecule	11658	-1.7	-6.5
	Aoc3	amine oxidase, copper containing 3	11754	-2.3	-3.1
	Efemp1	epidermal growth factor-containing fibulin-like extracellular matrix protein 1	216616	-1.0	-7.2
	Itgb8	PREDICTED: integrin beta 8 [Mus musculus], mRNA sequence	320910	-2.0	-1.0
	Myom1	myomesin 1	17929	-2.1	-3.2
	Pcdhb22	Protocadherin beta 22 (Pcdhb22), mRNA	93893	-1.8	-3.2
	Podxl	podocalyxin-like	27205	-1.3	-3.3
Proteolysis	1700112C13Rik	RIKEN cDNA 1700112C13 gene	74306	1.6	1.5
	2210010C04Rik	RIKEN cDNA 2210010C04 gene	67373	1.4	1.0
	2310051M13Rik	RIKEN cDNA 2310051M13 gene	70202	1.3	4.2
	4930486L24Rik	RIKEN cDNA 4930486L24 gene	214639	2.2	2.6
	4930519F16Rik	RIKEN cDNA 4930519F16 gene	75106	1.2	1.4
	4930523C11Rik /// Adam6	RIKEN cDNA 4930523C11 gene /// a disintegrin and metallopeptidase domain 6	238405	1.4	3.3
	4931440B09Rik	RIKEN cDNA 4931440B09 gene	71003	3.2	1.1
	9930032O22Rik	RIKEN cDNA 9930032O22 gene	320454	2.9	4.0
	Adamts4	a disintegrin-like and metallopeptidase (reprolysin type) with thrombospondin type 1 motif, 4	240913	1.3	1.2
	Anpep	alanyl (membrane) aminopeptidase	16790	1.8	4.9
	C2	complement component 2 (within H-2S)	12263	2.6	4.6
	Casp1	caspase 1	12362	2.1	2.0
	Cpz	carboxypeptidase Z	242939	2.3	2.3
	Dpp7	dipeptidylpeptidase 7	83768	1.5	1.2
	F11	coagulation factor XI	109821	1.4	2.9
	Gzmg	granzyme G	14944	1.1	2.1
	Klk13	kallikrein 13	13647	1.9	2.9
	Klkb1	kallikrein B, plasma 1	16621	1.1	3.1
	Mcpt4	mast cell protease 4	17227	1.3	1.9
	MGI:2665280	testis serine protease 2	235628	4.7	1.7
	Mme	membrane metallo endopeptidase	17380	1.6	3.0
	Plg	plasminogen	18815	2.7	1.8
	Prss28	protease, serine, 28	114661	1.2	1.9
	Prss35	protease, serine, 35	244954	1.1	2.3
	Tll1	tolloid-like	21892	2.5	2.8
	1700020H15	hypothetical protein 1700020H15 (1700020H15), mRNA	232717	-1.0	-2.3
	1810009J06Rik	RIKEN cDNA 1810009J06 gene	73626	-1.3	-1.1
	Adam11	a disintegrin and metallopeptidase domain 11	11488	-2.1	-1.1
	Cpa5	carboxypeptidase A5	74649	-1.6	-2.0

Proteolysis	Dpep3	dipeptidase 3	71854	-1.2	-3.7
	Klk12	kallikrein 12	69511	-2.4	-1.9
	Lect2	leukocyte cell-derived chemotaxin 2	16841	-2.4	-1.3
	Mcpt8	mast cell protease 8	17231	-1.2	-4.3
	Phex	phosphate regulating gene with homologies to endopeptidases on the X chromosome (hypophosphatemia, vitamin D resistant rickets)	18675	-2.6	-5.1
	Prss27	protease, serine 27	213171	-2.5	-2.3

*[1] Gene expression profiles in P29mtA11 and A11mtA11 were compared with those of P29mtP29 and A11mtP29, respectively (P29mtA11/P29mtP29 and A11mtA11/A11mtP29). Genes that expressed more than 200% upregulation or less than 50% downregulation were selected, and those associated with glycolysis pathway (including glucose transport), angiogenesis, apoptosis, cell adhesion, and proteolysis, which are essential for metastatic processes, were listed.

*[2] Since the magnitude of the changes is presented in logarithmic display, the expression of *Mcl-1* in high metastatic P29mtA11 and A11mtA11 cybrids is 2.0 and 3.2 times higher than in low metastatic P29mtP29 and A11mtP29 cybrids, respectively.

Supporting References

S1. J. W. Littlefield, *Exp. Cell Res*. **41**, 190 (1966).

S2. Y. Bai, G. Attardi, *EMBO J*. **17**, 4848 (1998).

S3. R. Acin-Perez *et al.*, *Hum. Mol. Genet.* **12**, 329 (2003).

S4. S. Hyuga *et al.*, *Cancer Res*. **54**, 3611 (1994).

S5. J. Jainchill, S. A. Aaronson, G. J. Todaro, *J. Virol.* **4**, 549 (1969).

S6. K. Inoue, *et al.*, *Nat. Genet.* **26**, 176 (2000).

S7. J-I. Hayashi, *et al.*, *Proc. Natl. Acad. Sci. USA* **88**, 10614 (1991).

S8. J.-I. Hayashi, *et al*., *J. Biol. Chem.* **269**, 19060 (1994).

S9. S. Miyabayashi *et al*., *J. Inher. Metab. Dis.* **12**, 373 (1989).